OPEN ACCESS
Thermophysics & Energy ARTICLE

Integrated cooling and power generation system addressing thermal protection and long-term power supply demands for scramjets: A novel design approach

Mingzhe Yu,[1] Jian Li,[1,*] Yunfei Zhang,[1] Xingying Chen,[2] and Jun Shen[1]
*Correspondence: lijian2022@bit.edu.cn
Received: February 7, 2026; Accepted: June 8, 2026; Published Online: July 20, 2026; https://doi.org/10.59717/j.xinn-energy.2026.100172

GRAPHICAL ABSTRACT

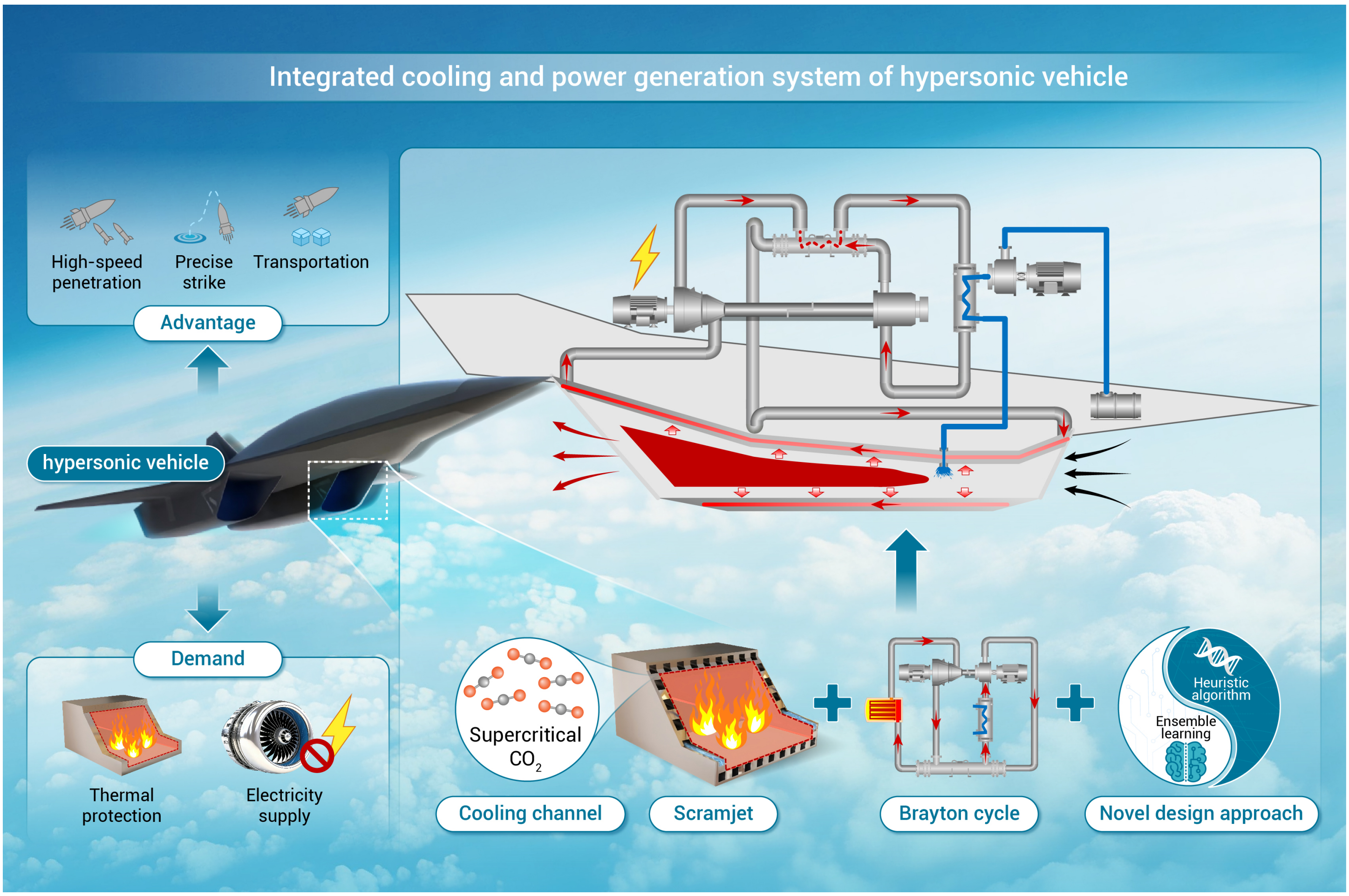

PUBLIC SUMMARY

- An integrated cooling and power generation system is designed for the scramjet.
- A novel design approach is proposed to achieve the optimal all-condition performance.
- A new rapid design method is developed based on Bayesian-optimized XGBoost model.
- Novel design approach enhances the average power generation efficiency by 21.59%.
- New rapid design method reduces the time use by 96.88% with an acceptable accuracy.

Integrated cooling and power generation system addressing thermal protection and long-term power supply demands for scramjets: A novel design approach

Mingzhe Yu,[1] Jian Li,[1,*] Yunfei Zhang,[1] Xingying Chen,[2] and Jun Shen[1]
[1]School of Mechanical Engineering, Beijing Institute of Technology, Beijing, 100081, China
[2]School of Electrical and Power Engineering, Hohai University, Nanjing 210024, China
*Correspondence: lijian2022@bit.edu.cn

Received: February 7, 2026; Accepted: June 8, 2026; Published Online: July 20, 2026; https://doi.org/10.59717/j.xinn-energy.2026.100172

Citation: Yu M., Li J., Zhang Y., et al. (2026). Integrated cooling and power generation system addressing thermal protection and long-term power supply demands for scramjets: A novel design approach. *The Innovation Energy* **3**:100172.

Hypersonic vehicles represent a new strategic frontier in aerospace technology, with the scramjet as their mainstream propulsion system. However, the scramjet presents significant challenges in thermal protection and electricity supply due to the long-term high-Mach-number operation and the lack of power drive shaft. Designing integrated cooling and power generation systems (ICPGSs) based on the supercritical CO_2 Brayton cycle can effectively solve these problems, with the advantages of high efficiency, compactness and non-coking. Nonetheless, its long-term operation under off-design conditions deviates from the rated-design condition. A novel integrated design approach is proposed by combining ensemble learning with heuristic algorithms to ensure a truly optimal all-condition performance. Different from existing studies that treat off-design analysis as a post-hoc validation, this design approach embeds a feedback mechanism into the rated-design optimization through ensemble-learning-based surrogate models and a synchronous iterative optimization of design and operation through heuristic algorithms, resulting in an improvement of up to 21.59%, which yields both a lower heat dissipation load and a larger electricity supply capacity. To reduce the unacceptable time consumption of numerical solutions in the optimization process, six surrogate models are considered and compared. A rapid design method based on a Bayesian-optimized XGBoost model is proposed, which enables a rapid and accurate prediction of system performance under diverse conditions, with the reduction in time consumption reaching up to 96.88%, and the mean absolute percentage error being only 1.59%. The findings provide theoretical support for the optimal design of ICPGSs and the performance enhancement of scramjets.

INTRODUCTION

Hypersonic vehicles have become a new strategic high ground in the development of aerospace technology since the 21st century.[1,2] Characterized by speeds exceeding Mach 5 within or beyond the atmosphere, they hold significant strategic value and broad application prospects in areas such as high-speed penetration, long-range precision strike, and rapid global reach.[3-5] When hypersonic vehicles undergo prolonged, high-Mach-number flight in near-space environments, the high-enthalpy inflow and combustion heat release subject scramjets to severe thermal conditions.[6-8] When the hypersonic vehicle reaches a flight Mach number of 7, the combustor temperature of the scramjet can reach as high as 2000 K.[9] This leads to a sharp temperature rise in the engine walls with prolonged flight time, readily causing structural damage and potentially resulting in mission failure.[10] Effective thermal protection technology for scramjets is of vital importance to the development of hypersonic vehicles.[11-13]

Thermal protection technology mainly includes passive thermal protection and active thermal protection.[14,15] Passive thermal protection refers to the use of lightweight, high-temperature-resistant materials to ensure the engine structure remains intact. However, as flight duration and Mach number increase, engine wall temperatures will exceed the materials' operational limits, making it difficult to meet thermal protection requirements.[16] Active thermal protection primarily relies on regenerative cooling technologies, utilizing hydrocarbon fuel flowing through cooling channels on the engine walls to provide thermal protection. However, during high-Mach-number flight, the fuel required for regenerative cooling exceeds combustion demands. Additionally, hydrocarbon fuels are prone to cracking, producing complex decomposition products that readily cause carbon deposits and coking within the cooling channels. This degrades heat transfer efficiency, posing significant challenges to the application of regenerative cooling technology.[17,18]

Beyond the cooling challenges of scramjets, hypersonic vehicles' various control and functional systems require significant electricity. However, the absence of rotating components in a scramjet rules out the conventional approach of using a shaft to drive a generator.[19] The prevailing solution of carrying batteries faces a fundamental limitation: the accumulating battery mass and volume with extended flight time become prohibitive in practice.[20,21] Achieving sustained, high-power electrical output is key to meeting the electricity requirements of long-duration flight.

An integrated cooling and power generation system (ICPGS) based on the supercritical CO_2 Brayton cycle not only converts heat into electricity for hypersonic vehicles but also satisfies the cooling demand of scramjets, thereby achieving simultaneous power generation and thermal protection with significant potential.[22] As a working fluid, CO_2 offers stable properties without being prone to thermal decomposition or coking. The Brayton cycle provides high thermal efficiency, which lowers the cooling demand on the fuel, along with a compact structure suitable for integration into hypersonic vehicles.[23,24] The performance superiority of ICPGSs has been verified. Guo et al.[25] proposed a novel ICPGS for hypersonic vehicles operating at Mach 6-7, designed to meet the cooling demand and prevent coking or failure in the engine wall cooling channels. Simultaneously, the electricity generated by the system can offset the performance penalty imposed on the hypersonic vehicle by the system's own additional weight. Miao et al.[23] proposed an ICPGS that can reduce fuel consumption for cooling by 28.8% compared with the conventional regenerative cooling system and output 159.5 kW. Furthermore, ICPGS can also be combined with additional arrangements, thereby giving rise to other forms. Cheng et al.[26,27] proposed a novel liquid metal magnetohydrodynamic enhanced ICPGS that can theoretically meet the megawatt-class electricity demand of hypersonic vehicles, achieving a power output of 637.84 kW per unit fuel mass flow rate with a maximum relative increase of 92.44% compared with the standalone. Wang et al.[28] proposed an ICPGS combining closed Brayton cycle with Rankine cycle via a heat exchanger, resulting in an increase of 6.2% in thermal efficiency and 16.59 kW in power generation compared with the standalone.

However, the actual flight mission of hypersonic vehicles involves multiple stages, takeoff, climb, cruise, speed change, descent, and landing, during which the temperature and heat flux on the engine walls fluctuate significantly.[29] Zhang et al.[30] found that the temperature and heat flux on the engine wall surface exhibited significant axial variations, which in turn affected the cooling system. Jason et al.[31] measured temperatures and heat flux densities within a scramjet combustor under simulated Mach 5 flight conditions using direct-write temperature sensors. Results indicated that during different flight stages, the differences in the wall temperature and heat flux density exceeded 400 K and 75 $W \cdot cm^{-2}$, respectively.

The combustor temperature and heat flux density of the scramjet fluctuate significantly over time, which will further impact the heat source conditions on the engine walls. Consequently, the ICPGS will operate under off-design conditions for extended periods. For the supercritical CO_2 Brayton cycle, off-design performance will significantly deviate from that under the rated-design condition.[32] Analyses based solely on the rated-design condition will greatly overstate the system's true application potential. The off-design performance analysis is proposed for a more valuable evaluation of the system. Ma et al.[33] investigated the coupled off-design performance of a scramjet and an ICPGS under Mach 4-7 cruise conditions, where the differences in net power output and thermal efficiency can exceed 100 kW and 4 percentage points, respectively. Dang et al.[21] investigated the off-design performance of an ICPGS combined with a fuel vapor turbine, with a total power output ranging from 77.3 kW to 90.0 kW. However, the significant performance degradation under the off-design condition that has been found is not yet well resolved. The optimization method considering both under rated-design and off-design conditions is essential for practical application.

A suboptimal scheme under the rated-design condition may paradoxically yield better performance under off-design conditions, which can be attributed to the performance gap between design and off-design conditions. A scheme optimized for a single rated-design condition compromises off-design performance, which consequently constrains enhancements of the performance under all operating conditions. Consequently, the system's optimization scheme under the rated-design condition should be iteratively refined based on feedback from its performance under off-design conditions, thereby achieving optimal all-condition performance that encompasses both rated-design performance and off-design performance. Furthermore, the establishment of this feedback mechanism relies on a comprehensive investigation of the performance under all operating conditions. Considering the temporal scale differences between system design and operational stages, along with the time-consuming nature of solving off-design performance models, the time and computational resources required by the traditional traversal method to map the performance under all operating conditions to design parameters are unacceptable.[34] Therefore, it is urgently necessary to develop an approach incorporating a feedback mechanism, featuring both high computational accuracy and short processing time, to pursue the optimal design scheme and thermodynamic performance of the ICPGS under all operating conditions.

This study focuses on an ICPGS based on the supercritical CO_2 Brayton cycle, incorporating a novel integrated design approach achieving the all-condition optimization. This integrated design approach combines ensemble learning with heuristic algorithms to ensure a synchronous iterative optimization during design and operation stages, by accounting for the feedback effect of off-design operation characteristics on the rated-design optimization, thereby guaranteeing truly optimal all-condition performance. To reduce the unacceptably long computational time for numerical solutions in the optimization process, a new rapid design method is proposed based on the comparison of six surrogate models to enable rapid and accurate prediction of the system performance for diverse conditions. Unlike existing studies that treat off-design analysis as a post-hoc validation, this design approach embeds the feedback mechanism into the rated-design optimization through ensemble-learning-based surrogate models. The thermodynamic superiority of this design approach is evaluated by comparing its results with those from the traditional approach lacking the feedback effect. The findings provide theoretical support for the optimal design of ICPGSs and the performance enhancement of scramjets. The flowchart of the main research content in this study is shown in Figure 1.

MATERIALS AND METHODS

System modeling

An ICPGS is built based on the supercritical CO_2 Brayton cycle, aiming for scramjets cooling and electricity supply requirements of hypersonic vehicles. The system configuration and thermodynamic process are illustrated in Figure 2A. The system adopts the supercritical CO_2 as the working fluid, absorbing heat from the engine high-temperature walls (heat source) to transform CO_2 into a high-temperature and high-pressure state. The supercritical CO_2 expands through a turbine to generate electricity. A regenerator recovers part of the heat from the turbine exhaust. The remaining heat is then transferred at a lower temperature to the low-temperature fuel (cold source). The low-temperature supercritical CO_2 is pressurized by the compressor and then enters the regenerator and the engine wall cooling channel to continue absorbing heat. Meanwhile, the fuel preheated by the CO_2 enters the combustor for combustion. The system provides the thermal protection for the scramjet and ensures a sustainable electricity supply for hypersonic vehicles during extended flights. At the same time, the preheated fuel enhances the combustion efficiency.

Heat source modeling

Based on engine wall temperature and heat flux density data from a scramjet tested at Mach 5 conditions, the heat source condition characterization models are established.[31]

The characterization model for the wall temperature variation over time at the combustor outlet is:

$$T_{w,out}(t)=\begin{cases}0.0047502t^3-0.45747t^2+12.7962t+530.6189 & 0<x\leq 31\text{s}\\ -0.001455t^3+0.21856t^2-9.771t+774.2931 & 31\text{s}<x\leq 73\text{s}\\ 0.023447t^3-6.6262t^2+626.1927t-18861.2433 & 73\text{s}<x\leq 107\text{s}\end{cases} \quad (1)$$

where $T_{w,out}$ is the wall temperature at the combustor outlet, K; t is the operating time, s.

The characterization model for the wall heat flux density variation over time at the combustor outlet is:

$$q_{w,out}(t)=\begin{cases}0.00034034t^3-0.018782t^2+0.31306t+0.04884 & 0<t\leq 13\text{s}\\ 0.00020305t^3-0.012043t^2+0.16979t-1.0964 & 13\text{s}<t\leq 31\text{s}\\ -0.00026637t^2+0.028144t+0.18466 & 31\text{s}<t\leq 73\text{s}\\ -0.015365t^3+3.5518t^2-272.8564t+6969.2057 & 73\text{s}<t\leq 81\text{s}\\ -0.00025061t^3+0.077388t^2-8.0137t+280.1263 & 81\text{ s}<t\leq 107\text{s}\end{cases} \quad (2)$$

where $q_{w,out}$ is the wall heat flux density at the combustor outlet, $MW\cdot m^{-2}$.

This scramjet adopts a single-stage circular combustor design. The combustor walls can be modeled as a regular cylinder with a total length of 1 m and a diameter of 0.25 m for simplified analysis. The characterization models for the wall temperature and heat flux density along the axial direction are as follows:[33]

$$T_w(x)=\begin{cases}3347.2393x^2+454.7789x+406.7294 & 0<x\leq 0.2\text{m}\\ -988.963x^2+1397.831x+386.1395 & 0.2\text{m}<x\leq 0.6\text{m}\\ 317.3097x+683.1142 & 0.6\text{m}<x\leq 1\text{m}\end{cases} \quad (3)$$

$$q_w(x)=\begin{cases}-0.85237x+1.4951 & 0<x\leq 0.07\text{m}\\ -51.7509x^2+17.484x+0.40423 & 0.07\text{m}<x\leq 0.2\text{m}\\ -1.0145x^2+0.53902x+1.7995 & 0.2\text{m}<x\leq 0.4\text{m}\\ -0.85904x+2.1889 & 0.4\text{m}<x\leq 1.0\text{m}\end{cases} \quad (4)$$

where T_w is the engine wall temperature, K; q_w is the combustor wall heat flux density, $MW\cdot m^{-2}$; x is the axial position of the combustor, m, where x=1 m represents the combustor outlet. It is assumed that the combustor inlet temperature remains constant, the axial distribution of wall temperature changes at a constant proportion and the axial distribution of wall heat flux density changes at a constant amplitude with operating time.

Cold source modeling

The ICPGS adopts the hydrocarbon fuel of the scramjet as the cold source. The fuel has an average specific heat capacity of 2.6 $kJ\cdot kg^{-1}\cdot K^{-1}$, with an initial temperature of 295 K. The maximum fuel temperature is limited to no more than 650 K to prevent excessive fuel outlet temperatures from causing coking.[35]

Thermodynamic modeling of system

Rated-design condition. The ICPGS comprises engine wall cooling channel for heat absorption, a radial-flow turbine, a centrifugal compressor, plate heat exchangers (recuperator and cooler), and other auxiliary equipment such as piping. The heat exchangers are in counterflow. The turbine and compres-

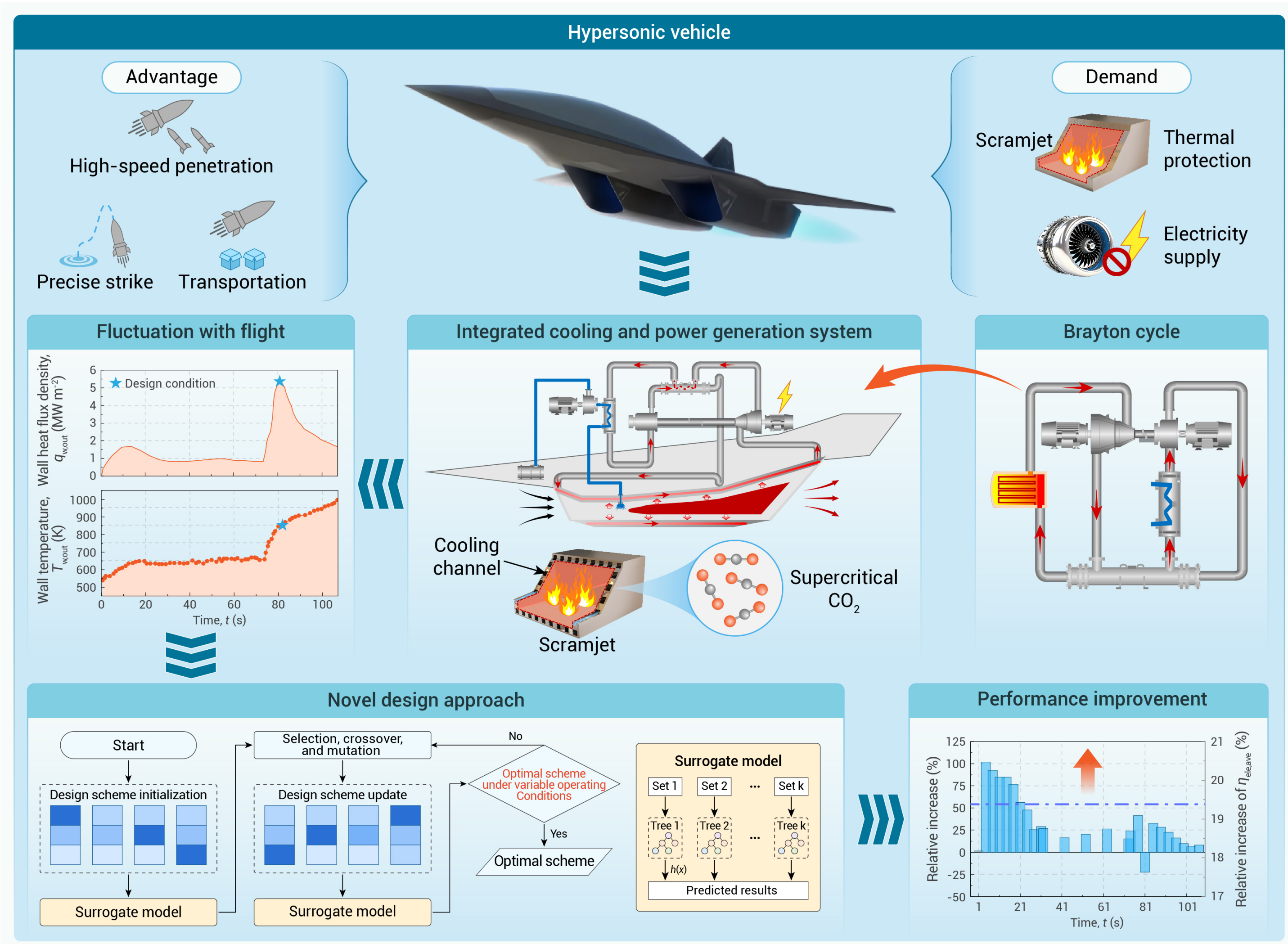

Figure 1. Flowchart of the main research content in this study.

sor adopt a coaxial configuration. The system modeling adopts the common assumptions for simplify analysis, as follows:[32,34]

- The heat losses of components and piping are negligible.
- The pressure drops through heat exchangers and piping are negligible.
- The changes in geopotential energy and kinetic energy of working fluid flowing through heat exchangers and piping are negligible.

The symbols in the equations are defined as: h for enthalpy, s for entropy, and m for mass flow rate. The subscript "s" is the ideal isentropic condition in the components. The η is the efficiency of the energy transfer process. The calculations for compressor isentropic efficiency and the power consumption are as follows:

$$\eta_{com} = \frac{h_{2s} - h_1}{h_2 - h_1} \tag{5}$$

$$W_{com} = \frac{m_{CO_2}(h_2 - h_1)}{\eta_m \eta_{mot}} \tag{6}$$

The calculation for turbine isentropic efficiency and the power output are as follows:

$$\eta_T = \frac{h_4 - h_5}{h_4 - h_{5s}} \tag{7}$$

$$W_T = m_{CO_2}(h_4 - h_5)\eta_m \eta_{gen} \tag{8}$$

The energy balance relationship of regenerator is as follows:

$$h_5 - h_6 = h_3 - h_2 \tag{9}$$

$$\delta = \frac{h_5 - h_6}{h_5 - h_1} \tag{10}$$

where δ is the regenerator efficiency, %.

The calculation of the heat absorption capacity is as follows:

$$Q_{in} = m_{CO_2}(h_4 - h_3) = \int_0^1 q_w(x)\pi d w dx \tag{11}$$

where d_w is the combustor diameter.

The calculation for the system heat release is as follows:[36]

$$Q_{cool} = m_{CO_2}(h_6 - h_1) = m_f c_{p,f}(T_{f1} - T_{f0}) \tag{12}$$

where $c_{p,f}$ is the average specific heat capacity of the fuel, kJ·kg^{-1}·K^{-1}; T_{f0} and T_{f1} are the temperatures of the fuel at the cooler inlet and outlet, respectively, K.

The parameter settings of the ICPGS are shown in Table S1. The thermophysical properties of CO_2 are sourced from REFPROP 10.0.

Because the engine wall temperature and heat flux density exhibit significant fluctuations and drastic variations in actual operation, the ICPGS operates under off-design conditions for extended periods. The off-design performance of the system is affected by the design scheme, which is formulated under the rated-design condition.[37]

Off-design condition. The calculation models for compressor isentropic efficiency are as follows:[38]

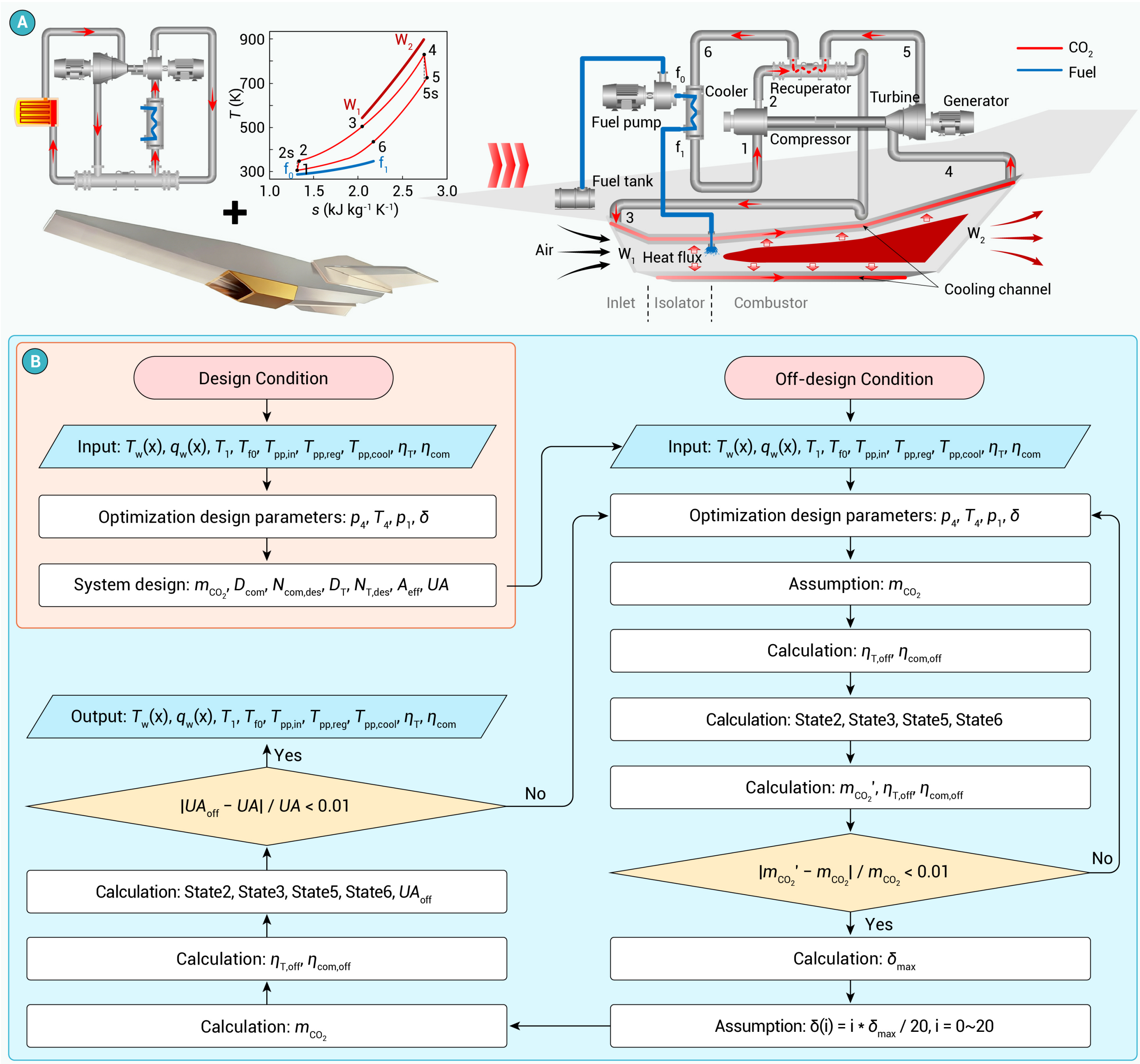

Figure 2. (A) An integrated cooling and power generation system based on supercritical CO_2 Brayton cycle. (B) Calculation flowchart of off-design performance.

$$\phi^*_{com} = \frac{m_{CO_2}}{\rho_{com,in} U_{com} D^2_{com}} \left(\frac{N_{com,off}}{N_{com,des}}\right)^{1/5} \tag{13}$$

$$U_{com} = \frac{D_{com}}{2} N_{com} \tag{14}$$

$$\psi^*_{com} = \frac{\Delta h_{com,is}}{U^2_{com,off}} \left(\frac{N_{com,des}}{N_{com,off}}\right)^{(20\phi^*_{com})^3} \tag{15}$$

$$\eta^*_{com} = \eta_{com,off} \left(\frac{N_{com,des}}{N_{com,off}}\right)^{(20\phi^*_{com})^5} \tag{16}$$

where ϕ^*_{com}, ψ^*_{com}, and η^*_{com} are the modified flow, ideal head, and efficiency coefficients, respectively; $\rho_{com,in}$ is the CO_2 density at the compressor inlet, kg·m^{-3}; U_{com} is the compressor impeller linear velocity, m·s^{-1}; D_{com} is the compressor impeller diameter, m; N_{com} is the compressor shaft speed, rad·s^{-1}; $\Delta h_{com,is}$ is the CO_2 specific enthalpy change in isentropic compression, kJ·kg^{-1}. The subscripts "des" and "off" represent the rated-design condition and the off-design condition, respectively. The correlations among ϕ^*_{com}, ψ^*_{com}, and η^*_{com} are as follows:

$$\psi^*_{com} = 0.04049 + 54.7\phi^*_{com} - 2505\phi^{*2}_{com} + 53224\phi^{*3}_{com} - 498626\phi^{*4}_{com} \tag{17}$$

$$\eta^*_{com} = -0.7069 + 168.6\phi^*_{com} - 8089\phi^{*2}_{com} + 182725\phi^{*3}_{com} - 1638000\phi^{*4}_{com} \tag{18}$$

The calculation models for turbine isentropic efficiency are as follows:[39]

$$m_{CO_2} = C_T A_{eff} \rho_{T,out} \tag{19}$$

$$\eta_{T,off} = \eta_{T,aero} \eta_{T,des} \tag{20}$$

$$\eta_{T,aero} = 2v\sqrt{1-v^2} \quad (21)$$

$$v = U_T / C_T \quad (22)$$

$$U_T = \frac{D_T}{2} N_T \quad (23)$$

$$C_T = \sqrt{2\Delta h_{T,is}} \quad (24)$$

where A_{eff} is the nozzle area, mm[2]; $\rho_{T,out}$ is the CO_2 density at the turbine outlet, kg·m^{-3}; $\eta_{T,aero}$ is the turbine aerodynamic efficiency; U_T is the turbine impeller linear velocity, m·s^{-1}; v is the ratio of U_T to the fluid spouting velocity C_T; D_T is the turbine impeller diameter, m; N_T is the turbine shaft speed, rad·s^{-1}; $\Delta h_{T,is}$ is the CO_2 specific enthalpy change in isentropic expansion, kJ·kg^{-1}. The correlations between $\eta_{T,aero}$ and v is as follows:

$$\eta_{T,aero} = 0.179921 + 1.3567v + 1.3668v^2 - 3.0874v^3 + 1.0626v^4 \quad (25)$$

The cooling demand of the ICPGS under off-design conditions can be satisfied via modulation of the fuel mass flow rate.

The regenerator modeling adopts the effectiveness-number of transfer unit (ε-NTU) method, divided into 30 sections with equal heat exchange capacity. The energy balance relationship of each section is as follows:[40]

$$Q_i = m_{hot}(h_{hot,in,i} - h_{hot,out,i}) = m_{cold}(h_{cold,out,i} - h_{cold,in,i}) \quad (26)$$

where the subscript "i" is the section number, and the subscripts "hot" and "cold" are the hot and cold sides of heat exchangers, respectively.

The calculation model for the effectiveness of the ith section and the number of transfer unit is as follows:[40]

$$\varepsilon_i = \frac{Q_i}{c_{p,\min,i}(T_{hot,in,i} - T_{cold,in,i})} \quad (27)$$

$$c_{R,i} = \frac{c_{p,\min,i}}{c_{p,\max,i}} \quad (28)$$

$$NTU_i = \begin{cases} \dfrac{\ln\left(\dfrac{1-\varepsilon_i c_{R,i}}{1-\varepsilon_i}\right)}{1-c_{R,i}} & c_{R,i} \neq 1 \\ \dfrac{\varepsilon_i}{1-\varepsilon_i} & c_{R,i} = 1 \end{cases} \quad (29)$$

where ε_i is the effectiveness; $c_{R,i}$ is the specific heat capacity ratio; NTU_i is the number of transfer unit; $c_{p,\min,i}$ and $c_{p,\max,i}$ are the minimum and maximum specific heat capacities of the fluids, respectively, kJ·kg^{-1}·K^{-1}; $T_{hot,in,i}$ and $T_{cold,in,i}$ are the inlet temperatures of the hot and cold fluids, K.

The calculation for the heat exchange performance coefficient of the ith section (UA_i) and for entire regenerator (UA) are as follows:

$$UA_i = NTU_i c_{p,\min,i} \quad (30)$$

$$UA = \sum_{i=1}^{30} UA_i \quad (31)$$

The calculation models of UA under design and off-design conditions are as follows:

$$\frac{1}{UA} \propto \frac{1}{m_{cold}{}^{0.8}} + \frac{1}{m_{hot}{}^{0.8}} \quad (32)$$

$$\frac{UA_{off}}{UA_{des}} = \frac{\dfrac{1}{m_{cold,des}{}^{0.8}} + \dfrac{1}{m_{hot,des}{}^{0.8}}}{\dfrac{1}{m_{cold,off}{}^{0.8}} + \dfrac{1}{m_{hot,off}{}^{0.8}}} = \left(\frac{m_{cold,off}{}^{0.8} m_{hot,off}{}^{0.8}}{m_{cold,des}{}^{0.8} m_{hot,des}{}^{0.8}}\right)\left(\frac{m_{cold,des}{}^{0.8} + m_{hot,des}{}^{0.8}}{m_{cold,off}{}^{0.8} + m_{hot,off}{}^{0.8}}\right) \quad (33)$$

Performance indexes. The calculation for the net power output of the ICPGS is as follows:[41]

$$W_{ele} = W_T - W_{com} \quad (34)$$

The calculation for the power generation efficiency of the ICPGS is as follows:

$$\eta_{ele} = \frac{W_{ele}}{Q_{in}} \quad (35)$$

Optimization process

Rated-design condition. A multi-parameter optimization of the ICPGS is performed using a genetic algorithm (GA) with maximizing power generation efficiency as the optimization objective. As the system absorbs a constant amount of heat, the operating condition for maximum power generation efficiency also yields the maximum power output. The optimization parameters are as follows:

- p_4: heat absorption pressure/MPa
- T_4: turbine inlet temperature/K
- p_1: heat release pressure/MPa
- δ: regenerator efficiency

The optimization model for maximizing power generation efficiency is as follows:

$$\begin{cases} f(x) = \max(\eta_{ele}) \\ x = \{p_4, T_4, p_1, \delta\} \\ x \subseteq R \end{cases} \quad (36)$$

where R is the range of values for the optimization design parameters. The boundaries of optimization parameters are shown in Table S2. The hyperparameter settings of the optimization model are shown in Table S3.

Off-design condition. The calculation flowchart of off-design performance is shown in Figure 2B. Performance calculations under off-design conditions are based on the rated-design condition. First, through GA optimization, the design scheme under rated-design condition is obtained, including heat absorption pressure, turbine inlet temperature, heat release pressure, regenerator efficiency, and CO_2 mass flow rate. Subsequently, the maximum power generation efficiency under the rated-design condition is also obtained. The design parameters for each system component are determined, including the compressor structure parameters and shaft speed, the turbine geometric parameters and shaft speed, and the regenerator heat transfer coefficient UA. Finally, the system design parameters are input into the performance calculation model under off-design conditions. Performance optimization is then conducted based on fluctuating heat source conditions to obtain the operating parameters and thermodynamic performance that satisfy various constraints under off-design conditions.

Model validation

The relative deviation (RD) is as follows:

$$RD = \frac{|Value_{ref} - Value_{cal}|}{Value_{ref}} \times 100\% \quad (37)$$

where $Value_{ref}$ is the reference value; $Value_{cal}$ is the calculation value.

The model in this study is validated against the results in Ref. [42], with the comparison detailed in Table S4. The results from the proposed model agree well with those reported in the literature.

RESULTS AND DISCUSSION

Concept of all-condition performance: Case study as an example

The concept of all-condition performance is proposed to describe the performance characteristics of the ICPGS under complex and diverse operating conditions. All-condition performance encompasses both rated-design performance and off-design performance. The system is designed under the rated-design condition, The ICPGS operates under off-design conditions for extended periods because of variations of wall temperature and heat flux density. its off-design performance is significantly affected by the design scheme and significantly deviates from the rated-design performance. The design process typically follows the traditional design approach, which focuses optimization solely under rated-design condition and fails to account

Table 1. Design scheme for the system and its components.

Design parameters	Value
Heat absorption pressure, p_4/MPa	19.99
Turbine inlet temperature, T_4/K	534.11
Heat release pressure, p_1/MPa	9.217
regenerator efficiency, δ	0.45
CO_2 mass flow rate, m_{CO2}/kg·s^{-1}	22.3074
Compressor impeller diameter, D_{com}/m	0.0846
Compressor shaft speed, $N_{com,des}$/rad·s^{-1}	4619
Turbine impeller diameter, D_T/m	0.118
Turbine shaft speed, $N_{T,des}$/rad·s^{-1}	4619
Effective nozzle area, A_{eff}/mm^{-2}	525.63
Heat exchange performance coefficient during heat absorption process, $UA_{in,des}$/kW·K^{-1}	54.02
Heat exchange performance coefficient of regenerator, $UA_{reg,des}$/kW·K^{-1}	88.35
Heat exchange performance coefficient of cooler, $UA_{cool,des}$/kW·K^{-1}	196.03

for the feedback effect from the off-design operation characteristics.

The fluctuation characteristics of heat source condition are confirmed based on the characterization model. The variations of wall temperature and heat flux density at the outlet of the combustor with time are shown as Figure 3A. Changes in heat flux density further induce fluctuations in the wall temperature. Due to the influence of thermal resistance and the heat capacity of the combustor wall material, changes in the wall temperature exhibit a certain degree of lag compared to heat flux density variations. Due to the continuous accumulation of wall heat flux density, the engine wall temperature exhibited an overall upward trend over time during the operating condition. Based on the fluctuation characteristics of heat source conditions, 25 representative operating condition points are selected for analyzing the all-condition performance of the ICPGS. The selection criteria are designed to capture the typical stages of the flight mission: the climb phases (stage 1), the stable cruise phases (stage 2), and the ramping phases (stage 3) where conditions change rapidly. This ensures that the all-condition performance analysis encompasses all key operational characteristics. To ensure the safe operation of the scramjet and prevent the combustor wall ablation under high heat flux density, the operating condition point with the maximum heat flux density is defined as the rated-design condition, namely point 18 (81 s).

Based on the rated-design optimization results of the ICPGS, design scheme for the system and its components are obtained, as shown in Table 1.

All-condition operating parameters of the ICPGS are shown in Figure 3B-E. The fluctuations in heat absorption pressure, heat release pressure, and regenerator efficiency over time are relatively minor compared to their optimization boundaries. The variations in turbine inlet temperature over time exhibit greater fluctuations. Both regenerator efficiency and turbine inlet temperature deviate significantly from their design values. Under all operating conditions, the heat absorption pressure approaches the optimal upper limit, fluctuating within the range of 18.50 to 20.00 MPa. The heat release pressure fluctuates within the range of 9.1 to 9.5 MPa. These parameters show a relatively small difference from their design values. The variation of regenerator efficiency with flight time fluctuates within the range of 0.1 to 0.15, which is much lower than its designed value of 0.45. The turbine inlet temperature of the system is close to the upper limit of optimization. These parameters deviate significantly from their design values. The reason for this phenomenon lies in the fact that the heat flux density of the engine wall fluctuates greatly with the flight time, causing significant changes in the heat absorption process of the system, as well as the heat exchange capacity of the regenerator and cooler. To meet the *UA* constraints of each heat exchange component and maintain a high-power generation efficiency under all operating conditions, the turbine inlet temperature and regenerator efficiency should be used as the main control parameters, which fluctuate with the flight time and deviate significantly from the design value. Moreover, influenced by the wall temperature of the engine, the deviation of the turbine inlet temperature is even greater.

Off-design performance of ICPGS is shown in Figure 3 F & G. The red dotted line chart illustrates how system rated-design performance varies with changes in design parameters. As system design parameters deviate from the optimal results, rated-design performance gradually declines. At this point, system performance is solely influenced by the design parameters. The higher heat absorption pressure, the greater the difference between its average heat absorption temperature and average heat release temperature, thereby enhancing the power generation efficiency. The power generation efficiency first increases and then decreases with rising heat release pressure. This pattern results from the competing effects of increased regenerator efficiency and elevated average heat release temperature. The outlet temperature of the compressor decreases as the heat release pressure increases. The upper limit of heat that the CO_2 preheating process can accommodate before entering the cooling channel increases. This leads to a rise in the maximum recoverable heat and an improvement in power generation efficiency. Simultaneously, the average heat release temperature will also increase. When the influence of the latter gradually outweighs that of the former, the power generation efficiency will decrease. As operating parameters gradually deviate from rated-design conditions, the off-design performance will deteriorate. This is the result of the combined effects of parameter variations and component efficiency. The deterioration degree of the off-design performance from rated-design performance decreases as the design parameters gradually deviates from the optimal results under the rated-design conditions. Compared to the heat absorption pressure, the off-design performance is more sensitive to the heat release pressure.

All-condition performance of the ICPGS is shown in Figure 3H. The power generation efficiency is 16.76% under the rated-design condition, while it drops to 2.63% under off-design conditions. Within Stage 1 and Stage 2, the power generation efficiency of the ICPGS remains at a relatively low level. This is due to the significant deviation of the heat source conditions in Stage 1 and Stage 2 from the rated-design condition. Consequently, the operating parameters deviate markedly from the design values, leading to a reduction in the power generation efficiency. In Stage 1, the operation of the ICPGS is affected by the coupling effect of the temperature and heat flux density of the engine wall, resulting in significant fluctuations in the power generation efficiency. In Stage 2, the heat source conditions remained relatively stable, and the power generation efficiency shows relatively small fluctuations. In Stage 3, the power generation efficiency rises to a maximum value under the rated-design condition before decreasing. The average power generation efficiency

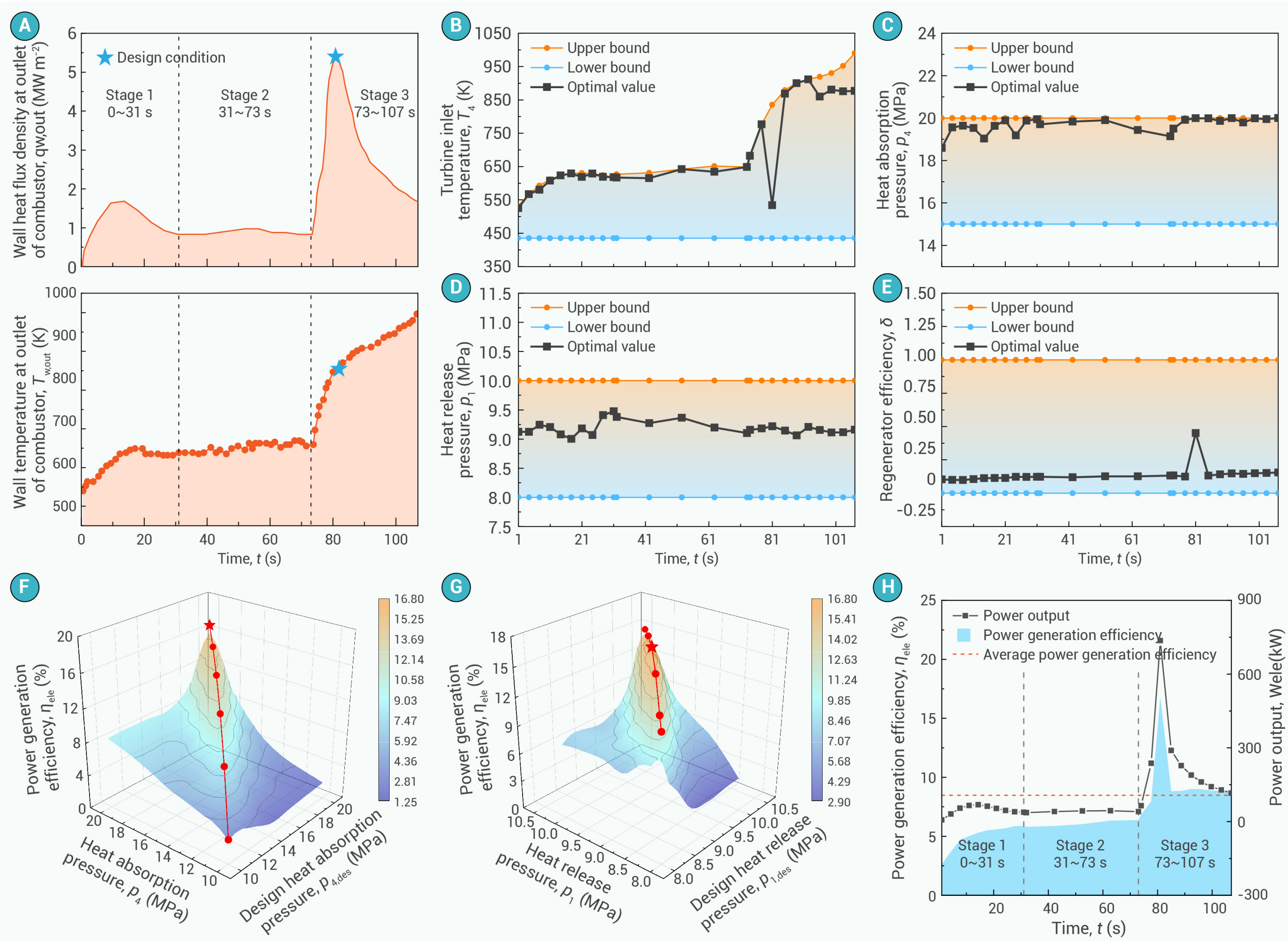

Figure 3. (A) Variations of wall temperature and heat flux density at the outlet of the combustor with time. (B-E) All-condition operating parameters of the integrated cooling and power generation system. Off-design performance of integrated cooling and power generation system of (F) Heat absorption pressure and (G) Heat release pressure. (H) All-condition performance of the integrated cooling and power generation system.

under all operating conditions is 8.48%. The entire combustor wall is used as the cooling object, and the outlet temperature is relatively low (about 407 K), which results in low efficiency but relatively high-power generation. The overall variation trend of the power generation under all operating conditions of the ICPGS is similar to that of the heat flux density.

In summary, the off-design performance is significantly affected by the design scheme and significantly deviates from the rated-design performance. Turbine inlet temperature is the key parameter for all-condition performance, as its temporal variations exhibit greater fluctuations compared to absorption pressure, heat release pressure, and regenerator efficiency. When parameters deviate from their optimal values, the performance deteriorates under both design and off-design conditions, while the performance gap between these two operating conditions narrows.

New rapid design method for all-condition optimization

This concept of all-condition performance enables the establishment of a mapping relationship between design parameters/schemes and system performance. However, the all-condition performance analysis must be conducted for each individual design scheme. Given that each scheme involves 3 design parameters, the total number of possible schemes can reach 100^3 or even 1000^3. This leads to an extremely high computational burden and prohibitively long computation times, rendering the direct approach infeasible. Therefore, a new rapid design method is developed based on a surrogate model. This method not only ensures the prediction accuracy but also significantly shortens the time consumption for optimization.

Employing surrogate models is a crucial strategy, particularly in scenarios involving complex simulations, high-dimensional design spaces, or costly experiments.[33,43,44] Dataset generation is a prerequisite for obtaining the surrogate model. The design parameter selection range covers the entire feasible optimization boundaries, as shown in Table S2. For the heat absorption pressure, the turbine inlet temperature, and the heat release pressure, an equidistant sampling method is adopted to generate a multi-dimensional parameter space. The regenerator efficiency is regarded as an optimization variable in the design process. Additionally, considering the requirement to obtain optimal performance for the system under all operating conditions, denser sampling is performed near higher values of average power generation efficiency (> 9%) within the parameter space. A total of 110 valid samples is obtained, as shown in Figure 4A.

Based on two current mainstream technical paths of surrogate models, including machine learning algorithms and traditional approximation methods, for the former, Back propagation neural network (BPNN), AdaBoost, XGBoost, and Random Forest (RF) are selected as potential model choices; for the latter, response surface models and Kriging are chosen. To fully exploit the optimal performance potential of machine learning algorithms, the hyperparameters of the four algorithms are optimized by the Bayesian algorithm. By constructing a probabilistic surrogate model to guide the search process, it can intelligently find the optimal hyperparameter combination with the minimum number of model evaluations, significantly reducing the computational cost caused by repeated model training. To ensure its generalization ability and considering that the acquisition of characteristics under

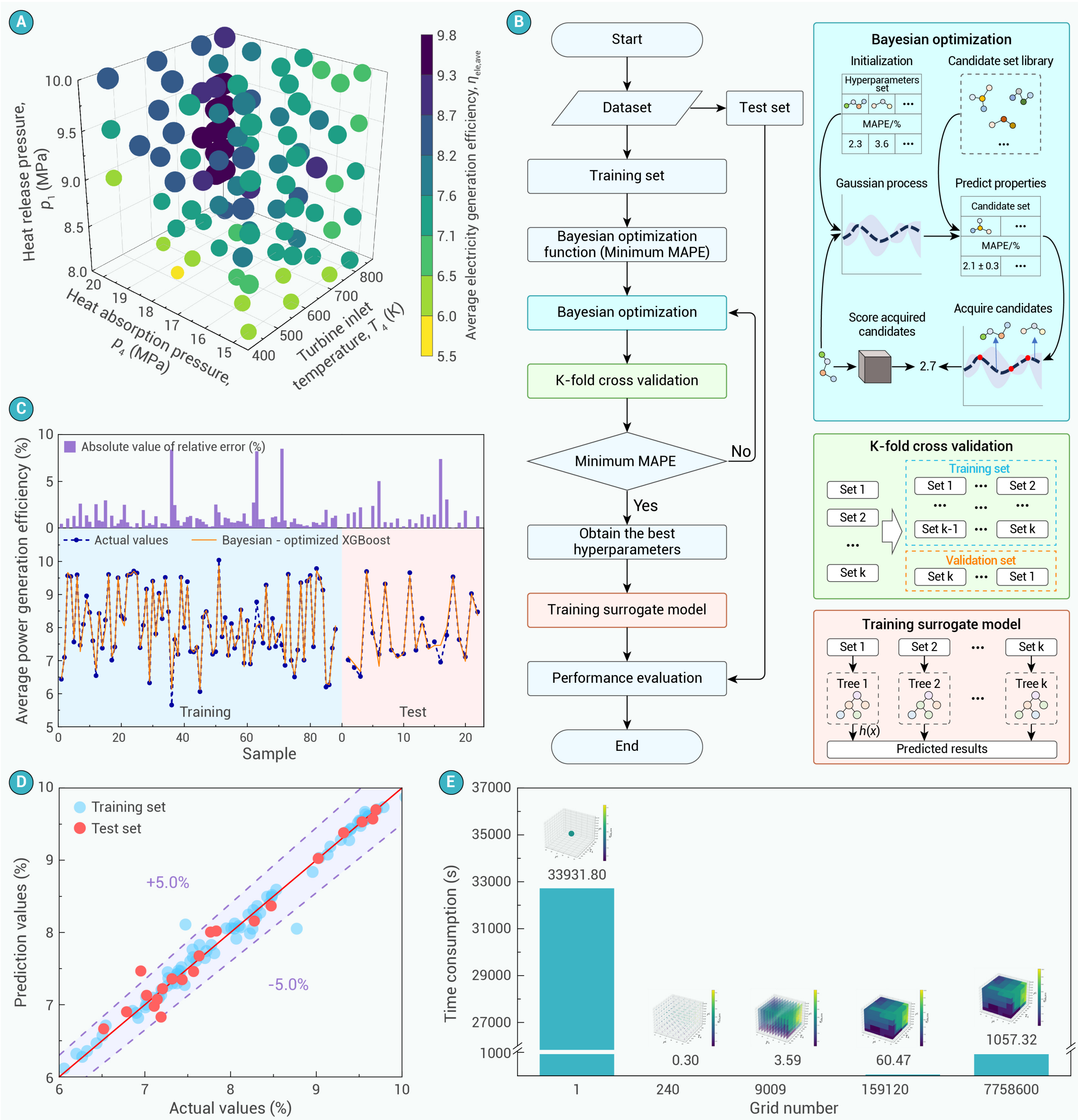

Figure 4. (A) Dataset used for the surrogate model. (B) Process of obtaining the surrogate model. (C & D) Mapping performance of average power generation efficiency based on Bayesian-optimized XGBoost model. (E) Time consumption for prediction of average power generation efficiency based on the Bayesian-optimized XGBoost model.

all operating conditions involves a significant amount of time-consuming work, the k-fold cross-validation method is adopted. It can repeatedly divide a limited and valuable data sample into training sets and validation sets. The evaluation results obtained through this method can more reliably reflect performance of the model on unknown data, effectively preventing the bias caused by overfitting to a specific data partition. The collaborative application of Bayesian optimization and k-fold cross-validation can build a highly accurate and reliable surrogate model for subsequent optimization tasks. Taking RF as an example, the process of obtaining the surrogate model is shown in the Figure 4B.

The performance of surrogate models is evaluated using mean absolute percentage error (MAPE), R-squared (R^2), mean square error (MSE), and root mean square error (RMSE). Lower values of MAPE, MSE and RMSE, along with higher R^2, indicate better performance. The minimum MAPE is used as the objective function for Bayesian optimization. The calculations are as follows.[45,46]

$$\mathrm{MAPE} = \frac{1}{N}\sum_{i=1}^{N}\left|\frac{\hat{y}_i - y_i}{y_i}\right| \quad (38)$$

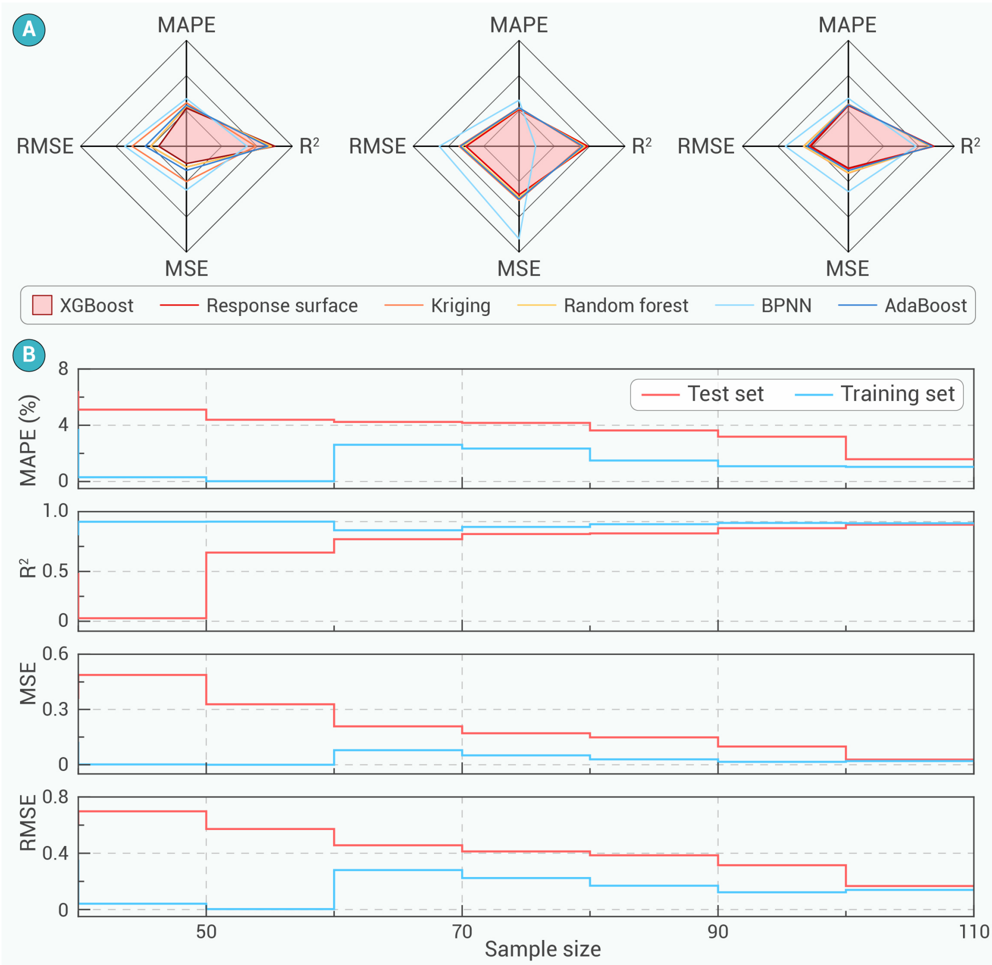

Figure 5. (A) Radar charts of surrogate models' performance comparison. (B) Learning curve of the surrogate model as the sample size changes.

$$R^2 = 1 - \frac{\sum_{i=1}^{N}(y_i - \hat{y}_i)^2}{\sum_{i=1}^{N}(y_i - \bar{y})^2} \tag{39}$$

$$MSE = \frac{1}{N}\sum_{i=1}^{N}(\hat{y}_i - y_i)^2 \tag{40}$$

$$RMSE = \sqrt{\frac{1}{N}\sum_{i=1}^{N}(\hat{y}_i - y_i)^2} \tag{41}$$

where N is the data size of test set or training set for the database; y_i is the actual value; $\hat{y}_i$ is the predicted value; $\bar{y}_i$ is the average value of test set or training set for the database.

In the training process of the surrogate models, 110 samples are divided into training and test sets with an 8:2 ratio. The k-fold cross validation (k=5) is used to prevent overfitting and ensure generalizability. Taking XGBoost as an example, the boundaries of optimization parameters are shown in Table S5. The hyperparameter settings of the Bayesian optimization are shown in Table S6.

Three random splits are conducted to evaluate the models' performance. The performance comparison across the six surrogate models is shown in Table S7, and radar charts of surrogate models' performance comparison are shown in Figure 5A. XGBoost achieves superior performance on the test set across different data splits, with the best values of MAPE, R^2, MSE, and RMSE being 1.59%, 0.9704, 0.0279, and 0.1671 respectively, and it is selected as the surrogate model.

Taking Bayesian-optimized XGBoost on data split 1 as an example, the learning curve of the surrogate model as the sample size changes is shown in Figure 5B. The prediction accuracy of the surrogate model increases with the sample size and comfortably meets the requirements when the sample size is 110.[47,48]

The mapping performance of average power generation efficiency based on Bayesian-optimized XGBoost model is shown in Figure 4C & D. The predicted values and actual values have a relatively high overall consistency. The relative errors of most samples are within the acceptable range. The model exhibits strong predictive performance and numerical stability. Although the relative errors of the test set are generally higher than those of the training set, the higher error values occur at the locations with lower average power generation efficiency. This is inessential for achieving a higher average power generation efficiency under all operating conditions when utilizing this model in subsequent optimization process.

The time consumption for prediction of average power generation efficiency based on the Bayesian-optimized XGBoost model is shown in Figure 4E. The model can significantly reduce the time consumption to obtain the average power generation efficiency. It only takes 1057.32 s to obtain data for a grid with a size of up to 7758600. Compared to the average 9.43 h (33931.80 s) used for the solution process of the performance model under all operating conditions that includes a rated-design condition and 24 off-design conditions, the reduction in time consumption can reach 96.88%.

In summary, six potential models based on the current mainstream technical paths of surrogate models are selected as potential choices. After the optimization using Bayesian optimization and the k-fold method. The Bayesian-optimized XGBoost model, selected after comparing four surrogate models, enables rapid and high-precision prediction of the ICPGS's all-condition performance, reducing the time consumption by 96.88% (with an acceptable MAPE of 1.59%) compared to direct numerical solutions.

Novel integrated design approach and its superiority evaluation

Based on the concept of all-condition performance and the rapid design method (the previously Bayesian-optimized XGBoost model), a novel integrated design approach optimizing all-condition performance of the ICPGS is presented, thus ensuring robust performance in actual operation and avoiding the discrepancy between excellent rated-design performance and poor off-design performance.

The flowchart of the novel integrated design approach is shown in Figure6A. Firstly, the genetic algorithm is used to initialize the design scheme. The rapid design method is called to quickly obtain the all-condition performance. Then, through the selection, crossover, and mutation processes, a new design scheme is generated, and rapid design method is called again to obtain the system performance and determine whether it has reached the optimal all-condition performance.

The optimization process and robust analysis for different data splits are shown in Figure 6B & C. The 95% confidence intervals for the average power generation efficiency from surrogate-assisted optimization ($\eta_{ele,ave,Sopt}$), numerical simulation ($\eta_{ele,ave,Num}$) and the relative deviation are [9.78%, 10.05%], [9.84%, 10.49%], and [0.56%, 4.47%], respectively, indicating narrow ranges and thus high precision of the predictions. Specifically, the relative deviation lies below the acceptable threshold of 5%,[43] confirming the reliability and robustness of the surrogate-assisted optimization process and results to different data splits. Based on the optimal all-condition optimization results, the optimal design scheme for the ICPGS system and its compo-

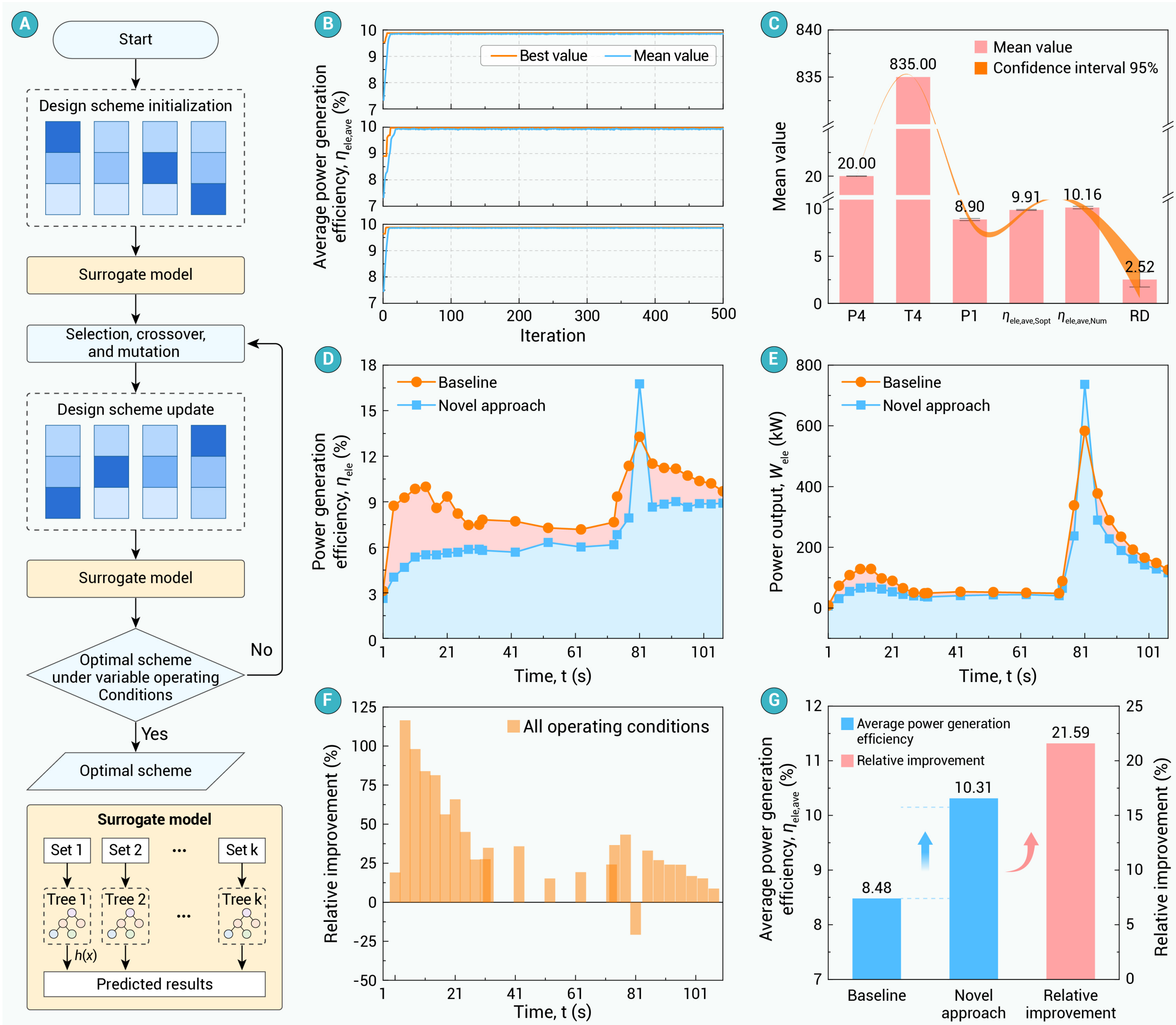

Figure 6. **(A) Flowchart of the novel integrated design approach. Surrogate-assisted optimization process and robust analysis to different data splits of (B) Optimization process and (C) Robust analysis. Comparison of (D) power generation efficiency under all operating conditions and corresponding (E) power output of the novel integrated design approach and the baseline. Relative improvement in power generation efficiency of the novel integrated design approach compared to the baseline. (D) Relative improvement under all operating conditions. (E) Relative improvement in average power generation efficiency.**

nents is obtained, as shown in Table 2.

Take the traditional design approach without the feedback effect as a baseline. The comparison of the power generation efficiency under all operating conditions and corresponding power output of this approach and the baseline is shown in Figure 6D & E. Under the rated-design condition, the power generation efficiency and power output of this approach are lower compared to those of the baseline. The power generation efficiency decreases from 16.76% to 13.28%, with a corresponding drop in power output from 736.41 kW to 583.31 kW. However, under off-design conditions, the power generation efficiency and power output of the approach both increases compared to the baseline. This indicates that as the flight time changes, the more intense the fluctuation of the heat source, the more pronounced the advantages of the proposed approach will be. Furthermore, this approach is more in line with the variation curve of the heat flux density of engine wall with flight time compared to the baseline, especially in Stage 1 and Stage 3. This promotes the improvement of the all-condition performance of the ICPGS.

The relative improvement (RI) in power generation efficiency is adopted as the evaluation index to assess the performance advantage of this approach over the baseline. The relative improvement in power generation efficiency is calculated as follows:[49]

$$\mathrm{RI} = \frac{\eta_{novel} - \eta_{baseline}}{\eta_{baseline}} \times 100\% \tag{42}$$

where η_{novel} is the power generation efficiency of the novel approach, %; $\eta_{baseline}$ is the power generation efficiency of the baseline, %.

The relative improvement in power generation efficiency of this approach compared to the baseline is shown in Figure 6 F & G. Under the rated-design condition, the power generation efficiency of this approach is 20.79% lower than that of the baseline; under the off-design conditions, the relative improvement of this approach can reach 8.73% to 116.48%. The average power generation efficiency of this approach is 8.48%, while that of the baseline system is 10.31%. The relative improvement in average power generation efficiency can reach 21.59%, effectively enhancing the all-condition

Table 2. Optimal design scheme for the system and its components.

Design parameters	Value
Heat absorption pressure, p_4/MPa	20.00
Turbine inlet temperature, T_4/K	835.00
Heat release pressure, p_1/MPa	8.78
regenerator efficiency, δ	0.16
CO_2 mass flow rate, m_{CO2}/kg·s^{-1}	7.68
Compressor impeller diameter, D_{com}/m	0.053
Compressor shaft speed, $N_{com,des}$/rad·s^{-1}	8158
Turbine impeller diameter, D_T/m	0.091
Turbine shaft speed, $N_{T,des}$/rad·s^{-1}	8158
Effective nozzle area, A_{eff}/mm^{-2}	245.86
Heat exchange performance coefficient during heat absorption process, $UA_{in,des}$/kW·K^{-1}	439.80
Heat exchange performance coefficient of regenerator, $UA_{reg,des}$/kW·K^{-1}	2.33
Heat exchange performance coefficient of cooler, $UA_{cool,des}$/kW·K^{-1}	48.50

performance of the ICPGS.

In summary, compared to the traditional approach, the novel integrated design delivers up to a 21.59% improvement in average power generation efficiency, with off-design efficiency gains ranging from 8.73% to 116.48%. It achieves this superior all-condition performance and a distinct optimal scheme, despite a slight trade-off in power generation efficiency and power output under the rated-design condition. This demonstrates that the overall performance gain far outweighs the limited, point-specific reduction.

CONCLUSION AND PROSPECTS

This study focuses on an ICPGS based on the supercritical CO_2 Brayton cycle for a scramjet, proposing a novel integrated design approach to ensure that the system possesses truly optimal all-condition performance. Addressing the issue of unacceptably high time consumption in the optimization process, a new rapid design method is proposed to enable rapid and accurate prediction of the system all-condition performance under complex and diverse operating condition, which is selected after comparing six surrogate models. Thermodynamic superiority of this design approach is evaluated. The main conclusions are summarized as follows:

- The novel integrated design approach achieves superior all-condition performance, offering up to a 21.59% higher average power generation efficiency than the traditional approach. This results not only in a reduced heat dissipation load for the scramjet but also in an enhanced electricity supply capacity for hypersonic vehicles.
- The scheme for optimal all-condition performance differs from that for optimal rated-design performance. While it sacrifices some rated-design performance, but this is offset by far superior off-design performance, with a relative improvement ranging from 8.73% to 116.48% under off-design conditions.
- A new rapid design method is developed based on the Bayesian-optimized XGBoost model, which enables rapid and high-precision prediction of the system's all-condition performance, reducing the time consumption by 96.88% (with an acceptable MAPE of 1.59%) compared to direct numerical solutions.
- Turbine inlet temperature is the key parameter affecting all-condition performance, whose temporal variations exhibit greater fluctuations compared to those of absorption pressure, heat release pressure, and regenerator efficiency.

This study is primarily based on theoretical analysis and numerical simulations due to the difficulty in obtaining published experimental data at present. Furthermore, the proposed design concept holds potential for extension to the optimization and design of other thermodynamic systems, and further verification is valuable. Future work will explore the possibilities of modifying the configuration or selecting only the high-temperature section to improve efficiency, using the all-condition optimization approach developed herein.

Nomenclature

A	Area (m^2)
C	Fluid spouting velocity (m·s^{-1})
c	Specific heat capacity (kJ·kg^{-1}·K^{-1})
D	Impeller diameter (m)
h	Enthalpy (kJ·kg^{-1})
m	Mass flow rate (kg·s^{-1})
N	Shaft speed (rad·s^{-1})
p	Pressure (MPa)
Q	Heat capacity (kW)
q	Heat flux density (MW·m^{-2})
T	Temperature (K)
U	Impeller linear velocity (m·s^{-1})
UA	Heat exchange performance coefficient (kW·K^{-1})
W	Power (kW)

Greek symbols

δ	Regenerator efficiency
ε	Effectiveness
η	Efficiency
v	Velocity ratio
ρ	Density
ϕ	Flow coefficient
ψ	Ideal head coefficient
Δ	Difference

Superscripts/Subscripts

1-10	State points

aero	Aerodynamic
ave	Average
cal	Calculation
com	Compressor
cool	Cooler
des	Design
ele	Electricity
f	Fuel
gen	Generator
m	Machine
mot	Motor
Num	Numerical simulation
off	Off-design
pp	Pinch point
ref	Reference
reg	Regenerator
Sopt	Surrogate-assisted optimization
T	Turbine
w	Wall
*	Modification

Abbreviations

ICPGS	Integrated Cooling and Power Generation System
RD	Relative Deviation
MAPE	Mean Absolute Percentage Error
MSE	Mean Square Error
RMSE	Root Mean Square Error
RI	Relative Improvement
NTU	Number of Transfer Unit

REFERENCES

1. Hu F., Wang J., Sui Z., et al. (2025). A review on research progress of large area thermal protection structures for hypersonic vehicles. *Acta Astronaut.* **232**:541–556. DOI:10.1016/j.actaastro.2025.04.006
2. Sheng Z., He Y., Wang S., et al. (2025). Dynamics, chemistry, and modeling studies in the aviation and aerospace transition zone. *Innovation* **6**:101012. DOI:10.1016/j.xinn.2025.101012
3. Shao C., Zhao H., Zhuang N., et al. (2025). Design and mechanical performance analysis of a flexible thermal protection structure for morphing hypersonic vehicles. *Aerosp. Sci. Technol.* **168**:110822. DOI:10.1016/j.ast.2025.110822
4. Xue Z., Wang C., Wang R., et al., (2025). Research on the performance of an integrated active cooling and propulsion system for hypersonic glide vehicles. *Energy* **337**:138363. DOI:10.1016/j.energy.2025.138363
5. Jin F., Wang Y., Pang D., et al. (2026). Numerical investigations on aerodynamic characteristics in a longitudinal V-shaped hypersonic vehicle formation. *Aerosp. Sci. Technol.* **168**:111249. DOI:10.1016/j.ast.2025.111249
6. Yu B., Zhou W., Qin J., et al. (2017). Dynamic characteristics of hydrocarbon fuel within the channel at supercritical and pyrolysis condition. *J. Therm. Sci.* **26**:560–569. DOI:10.1007/s11630-017-0974-z
7. Zhao Z., Chen X., Huang Y., et al. (2026). Coupling of isolator flow with heat release rate and equivalence ratio oscillations in the dual-mode scramjet. *Combust. Flame* **283**:114588. DOI:10.1016/j.combustflame.2025.114588
8. Sprunger J., La Sorsa A.J., Hytovick R., et al. (2025). Turbulent flame compressibility criterion for scramjet unstart and transition. *Combust. Flame* **274**:114044. DOI:10.1016/j.combustflame.2025.114044
9. Nakaya S.J., Tsue M.H., Kono M., et al. (2015). Effects of thermally cracked component of n-dodecane on supersonic combustion behaviors in a scramjet model combustor. *Combust. Flame* **162**:3847–3853. DOI:10.1016/j.combustflame.2015.07.021
10. Wang J., Zhong M., Li J., et al. (2025). Mitigating hypersonic heat barrier via direct cooling enhanced by leidenfrost inhibition. *Nat. Commun.* **16**:6931. DOI:10.1038/s41467-025-62120-2
11. Oliveira Júnior P.C., Arrais Bezerra S.I., Souza S.I.S., et al. (2025). Impact of wall cooling on the stability and aerothermodynamic performance of a scramjet inlet. *Appl. Therm. Eng.* **279**:128040. DOI:10.1016/j.applthermaleng.2025.128040
12. Zhou X., Zhang S., Zuo J., et al. (2025). Comparison of conjugate heat transfer characteristics between regenerative cooling and recooling system for a methane-fueled scramjet. *Energy* **336**:138569. DOI:10.1016/j.energy.2025.138569
13. Jiang T., Zhan T., Li Y., et al. (2025). Heat transfer characteristics and flow distribution behavior of pyrolytic ammonia in scramjet regenerative cooling channels. *Energy* **335**:138187. DOI:10.1016/j.energy.2025.138187
14. Zhang C., Qin J., Yang Q., et al. (2015). Design and heat transfer characteristics analysis of combined active and passive thermal protection system for hydrogen fueled scramjet. *Int. J. Hydrogen Energy* **40**:675–682. DOI:10.1016/j.ijhydene.2014.11.036
15. Gopinath N., Dan A., Aruna S.T., et al. (2024). High emittance plasma sprayed ZrO_2-Y_2O_3/$La_2Zr_2O_7$ thermal barrier coatings for potential application in scramjets. *Appl. Surf. Sci.* **652**:159324. DOI:10.1016/j.apsusc.2024.159324
16. Ma X., Jiang P. and Zhu Y. (2022). Performance analysis and dynamic optimization of integrated cooling and power generation system based on supercritical CO_2 cycle for turbine-based combined cycle engine. *Appl. Therm. Eng.* **215**:118867. DOI:10.1016/j.applthermaleng.2022.118867
17. Luo S., Xu D., Song J., et al. (2021). A review of regenerative cooling technologies for scramjets. *Appl. Therm. Eng.* **190**:116754. DOI:10.1016/j.applthermaleng.2021.116754
18. Zhou Q., Li Y., Xia J., et al. (2025). Effects of n-decane pyrolysis on supercritical jet impingement heat transfer employed in thermal management of scramjet engines. *Int. J. Heat Fluid Flow* **116**:109902. DOI:10.1016/j.ijheatfluidflow.2025.109902
19. Dang C., Cheng K., Xu J., et al. (2023). Performance analysis of a thermal management system based on hydrocarbon-fuel regenerative cooling technology for scramjets. *Energy* **285**:128720. DOI:10.1016/j.energy.2023.128720
20. Luo Q., Luo L., Xing H., et al. (2025). Performance evaluation of regenerative cooling and closed Brayton cycle for hypersonic vehicles. *Energy* **333**:137356. DOI:10.1016/j.energy.2025.137356
21. Dang C., Tan X., Xu J., et al. (2026). Off-design performance evaluation of a novel power and thermal management system for hypersonic vehicles: thermodynamic analysis, operating boundary optimization. *Appl. Therm. Eng.* **287**:129423. DOI:10.1016/j.applthermaleng.2025.129423
22. Ma X., Jiang P. and Zhu Y. (2024). Dynamic simulation and analysis of transient characteristics of a thermal-to-electrical conversion system based on supercritical CO_2 Brayton cycle in hypersonic vehicles. *Appl. Energy* **359**:122686. DOI:10.1016/j.apenergy.2024.122686
23. Miao H., Wang Z. and Niu Y. (2020). Performance analysis of cooling system based on improved supercritical CO_2 Brayton cycle for scramjet. *Appl. Therm. Eng.* **167**:114774. DOI:10.1016/j.applthermaleng.2019.114774
24. Wu W., Shen J., Kong H., et al. (2024). Energy system and resource utilization in space: A state-of-the-art review. *Innov. Energy* **1**:100029. DOI:10.59717/j.xinn-energy.2024.100029
25. Guo L., Pang L., Yang X., et al. (2023). A power and thermal management system for long endurance hypersonic vehicle. *Chin. J. Aeronaut.* **36**:29–40. DOI:10.1016/j.cja.2022.07.012
26. Cheng K. Wang Y., Xu J., et al. (2022). A novel liquid metal MHD enhanced Closed-Brayton-Cycle power generation system for hypersonic vehicles: Thermodynamic analysis and performance evaluation with finite cold source. *Energ. Convers. Manage.* **268**:116068. DOI:10.1016/j.enconman.2022.116068
27. Lang L., Fu Y., Jiang F., et al. (2025). Investigation the thermodynamic performance of closed Brayton cycle with CO_2-based binary mixtures for hypersonic vehicle power generation systems under finite cold source. *Them. Sci. Eng. Prog.* **63**:103714. DOI:10.1016/j.tsep.2025.103714
28. Wang L., Liu Y., Tang C., et al. (2025). Thermodynamic analysis of helium-xenon closed Brayton cycle combined with Rankine cycle power generation system for hypersonic vehicle. *Them. Sci. Eng. Prog.* **62**:103659. DOI:10.1016/j.tsep.2025.103659
29. Balland S., Fernandez V.V. and Steelant J. (2015). Thermal and energy management for hypersonic cruise vehicles - cycle analysis. *AIAA Int. Space Planes Hypers. Sys. Tech. Conf.* **3557**. DOI:10.2514/6.2015-3557
30. Zhang D., Yu F., Zhang S., et al. (2016). Quasi-one-dimensional model of scramjet combustor coupled with regenerative cooling. *J. Propul. Power* **32**:687–697. DOI:10.2514/1.B35887
31. Trelewicz J.R., Longtin J.P., Gouldstone C., et al. (2015). Heat flux measurements in a scramjet combustor using embedded direct-write sensors. *J. Propul. Power*

31:1003–1013. DOI:10.2514/1.B35585
32. Yang J., Yang Z. and Duan Y. (2020). Off-design performance of a supercritical CO_2 Brayton cycle integrated with a solar power tower. *Energy* 201:117676. DOI:10.1016/j.energy.2020.117676
33. Ma X., Shu Y., Zhao S., et al. (2025). Off-design performance analysis of a supercritical carbon dioxide Brayton cycle coupled with a scramjet based on deep learning method. *Energy* 341:139462. DOI:10.1016/j.energy.2025.139462
34. Hu S., Li J., Yang F., et al. (2020). How to design organic Rankine cycle system under fluctuating ambient temperature: A multi-objective approach. *Energ. Convers. Manage.* 224:113331. DOI:10.1016/j.enconman.2020.113331
35. Miao H., Che X., Geng T., et al. (2025). Coupled modeling and performance analysis of a supercritical CO_2 cycle cooling system integrated with the actively cooled combustor for scramjets. *Appl. Therm. Eng.* 280:128492. DOI:10.1016/j.applthermaleng.2025.128492
36. Miao H., Wang Z. and Niu Y. (2020). Key issues and cooling performance comparison of different closed Brayton cycle based cooling systems for scramjet. *Appl. Therm. Eng.* 179:115751. DOI:10.1016/j.applthermaleng.2020.115751
37. Yang J., Yang Z. and Duan Y. (2022). A review on integrated design and off-design operation of solar power tower system with S-CO_2 Brayton cycle. *Energy* 246:123348. DOI:10.1016/j.energy.2022.123348
38. Yu Y. and Li X. (2023). Selecting dry cooling system for supercritical carbon dioxide Brayton cycle: Thermoeconomic analysis. *Appl. Therm. Eng.* 220:119759. DOI:10.1016/j.applthermaleng.2022.119759
39. Dyreby J.J. (2014). Modeling the Supercritical Carbon Dioxide Brayton Cycle with Recompression. PhD thesis (University of Wisconsin-Madison).
40. Yang J., Yang Z. and Duan Y. (2020). Part-load performance analysis and comparison of supercritical CO_2 Brayton cycles. *Energ. Convers. Manage.* 214:112832. DOI:10.1016/j.enconman.2020.112832
41. Ma X., Guo H., Jiang P., et al. (2025). Performance analysis and design optimization of a supercritical CO_2 Brayton cycle cooling and power generation system coupled with a scramjet. *Appl. Energy* 383:125362. DOI:10.1016/j.apenergy.2025.125362
42. Miao H. (2021). Investigation on supercritical carbon dioxide cycle based thermoelectric conversion system for scramjet. PhD thesis (National University of Defense Technology).
43. Zhang Y., Li J., Yu M., et al. (2025). Dominant factor identification and fast optimization of carnot battery by integrating SHAP and physics-guided neural network. *Appl. Energy* 401:126641. DOI:10.1016/j.apenergy.2025.126641
44. Wang N., Chen Y. and Zhang D. (2025). A comprehensive review of physics-informed deep learning and its applications in geoenergy development. *Innov. Energy* 2:100087. DOI:10.59717/j.xinn-energy.2025.100087
45. Alruqi M., Sharma P. and Agbulut U. (2023). Investigations on biomass gasification derived producer gas and algal biodiesel to power a dual-fuel engines: Application of neural networks optimized with Bayesian approach and K-cross fold. *Energy* 282:128336. DOI:10.1016/j.energy.2023.128336
46. Xie B., Shi S., Liu W., et al. (2025). Integrated forecasting of marine renewable power: An adaptively Bayesian-optimized MVMD-LSTM framework for wind-solar-wave energy. *Sustain. Energy Technol. Assess.* 84:104753. DOI:10.1016/j.seta.2025.104753
47. Tian Z., Gan W., Zou X., et al. (2022). Performance prediction of a cryogenic organic Rankine cycle based on back propagation neural network optimized by genetic algorithm. *Energy* 254:124027. DOI:10.1016/j.energy.2022.124027
48. Hajialigol N., Fattahi A., Karimi N., et al. (2024). Hybridized power-hydrogen generation using various configurations of Brayton-organic flash Rankine cycles fed by a sustainable fuel: Exergy and exergoeconomic analyses with ANN prediction. *Energy* 290:130166. DOI:10.1016/j.energy.2023.130166
49. Yu M., Yang F., Zhang H., et al. (2024). Thermoeconomic performance of supercritical carbon dioxide Brayton cycle systems for CNG engine waste heat recovery. *Energy* 289:129972. DOI:10.1016/j.energy.2023.129972

FUNDING AND ACKNOWLEDGMENTS

This study was funded by National Natural Science Foundation of China (Nos. 52476001 and U22B20112), National Key R&D Program of China (No. 2024YFB4206800), Xplorer prize (XP202129), and Beijing Institute of Technology Research Fund Program for Young Scholars.

AUTHOR CONTRIBUTIONS

All authors contributed to and approved the final version of the manuscript.

DECLARATION OF INTERESTS

Jun Shen is an Editorial Board member of The Innovation Energy and was blinded from reviewing or making final decisions on the manuscript. Peer review was handled independently of this member and their research group. The other authors declare no conflicts of interest.

DATA AND CODE AVAILABILITY

The data that support the findings of this work are available from the corresponding author upon reasonable request.

SUPPLEMENTAL INFORMATION

It can be found online at: https://doi.org/10.59717/j.xinn-energy.2026.100172